JCTC Journal of Chemical Theory and Computation

Article

Cite This: J. Chem. Theory Comput. 2019, 15, 6617−6624

pubs.acs.org/JCTC

Relativistic Real-Time Time-Dependent Equation-of-Motion Coupled-Cluster

Lauren N. Koulias,[†] David B. Williams-Young,[‡] Daniel R. Nascimento,[¶] A. Eugene DePrince, III,*[,¶] and Xiaosong Li*[,†]

[†]Department of Chemistry, University of Washington, Seattle, Washington 98195, United States

[‡]Computational Research Division, Lawrence Berkeley National Laboratory, 1 Cyclotron Road MS 50A-3111, Berkeley, California 94720, United States

[¶]Department of Chemistry and Biochemistry, Florida State University, Tallahassee, Florida 32306, United States

ABSTRACT: We present a relativistic time-dependent equation-of-motion coupled-cluster with single and double excitations (TD-EOM-CCSD) formalism. Unlike other explicitly time-dependent quantum chemical methods, the present approach considers the time correlation function of the dipole operator, as opposed to the expectation value of the time-dependent dipole moment. We include both scalar relativistic effects and spin−orbit coupling variationally in this scheme via the use of the exact two-component (X2C) wave function as the reference that enters the coupled-cluster formalism. In order to evaluate the accuracy of X2C-TD-EOM-CCSD, we compare zero-field splitting in atomic absorption spectra of open-shell systems (Na, K, Mg^+, and Ca^+) with values obtained from experiment. In closed-shell species (Na^+, K^+, Mg^{2+}, and Ca^{2+}), we observe singlet−triplet mixing in the X2C-TD-EOM-CC calculations, which results from the use of the X2C reference. The effects of the X2C reference are evaluated by comparing spectra derived from X2C-TD-EOM-CC calculations to those from TD-EOM-CC calculations using a complex generalized Hartree−Fock (ℂ-GHF) reference.

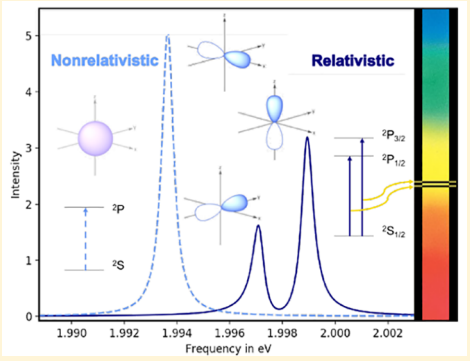

1. INTRODUCTION

Relativistic effects, including both scalar effects and spin−orbit coupling, have profound impacts on many photochemical processes. These effects are responsible for the manifestation of orbital contraction, increased binding energies, and intersystem crossing in molecular spectroscopies.[1−3] As such, a qualitatively correct theoretical description of the spectroscopy of heavy elements or of spin-forbidden processes requires full consideration of both scalar relativistic and spin−orbit coupling effects. Frequency-domain quantum chemical models built upon coupled-cluster (CC) theory,[4] such as the linear response (LR)[5,6] or equation-of-motion (EOM)[7−9] approaches, are highly accurate and widely used tools for modeling both valence- and core-electron absorption spectra.[10,11] Relativistic frequency-domain LR- and EOM-CC calculations provide highly accurate descriptions of spin−orbit splittings, photoelectron spectra, and other excited-state properties by incorporating relativistic effects through both perturbative[12−19] and variational treatments of spin−orbit couplings.[20−24]

While frequency-domain LR- and EOM-CC approaches have proven to be powerful tools for the excited-state problem, the response of a molecular system to an external perturbation can also be evaluated explicitly via integration of the time-dependent Schrödinger equation. Spectroscopic signals, such as the linear absorption spectrum, can be resolved by transforming quantum mechanical observables in the time domain to the frequency domain. Time-domain approaches are particularly advantageous when computing a broad-band spectrum of a molecular system,[25] resolving spectroscopic signatures of a region of high density of states,[26] or simulating nonequilibrium dynamics driven by a strong electromagnetic perturbation.[27] Such explicitly time-dependent approaches have become common at the Hartree−Fock and density functional theory levels (see ref 27 and references therein). On the other hand, simulations of correlated electron dynamics, particularly at the CC[28−32] and EOM-CC[33,34] levels of theory, are much more rare.

Given a time-dependent Hamiltonian operator, a time-dependent CC theory can be achieved by incorporating time dependence into the CC excitation amplitudes[29,32,35,36] and the underlying molecular orbital (MO) basis.[28,30,31,35,36] The MOs and CC amplitudes can then be evolved according to the time-dependent Schrödinger equation. However, because the CC wave function must satisfy a time-dependent bivariational principle,[30] the complete specification of the system at arbitrary times can be achieved only through the evolution of both the right-hand CC wave function, parametrized by the CC excitation amplitudes, and a left-hand CC wave function, which is defined in terms of both CC excitation and de-excitation amplitudes.[30−32] The CC de-excitation amplitudes

Received: July 21, 2019
Published: October 16, 2019

DOI: 10.1021/acs.jctc.9b00729
J. Chem. Theory Comput. 2019, 15, 6617−6624

also depend on time, and their time evolution is governed by the complex conjugate of the time-dependent Schrödinger equation. Moreover, the nonlinear nature of the cluster operator leads to complicated equations for the time evolution of the system. This latter complexity can potentially be avoided by holding the (de-)excitation amplitudes and orbitals fixed at their ground-state values and considering time evolution of the system only at the EOM-CC level of theory.[33,34,37,38] Indeed, refs 33 and 34 describe laser-driven electron dynamics modeled according to this prescription.

In this work, we employ a fundamentally different approach to time-dependent CC theory based not on the laser-induced time evolution of observables such as the dipole moment but, rather, on the time evolution of a field-free dipole autocorrelation function.[25,39] Unlike other time-dependent CC and EOM-CC approaches, which require the time evolution of both left- and right-hand CC wave functions, the moment-based formalism requires the explicit time evolution of only a single quantity: either the left-hand or right-hand CC dipole moment function. Specifically, we develop a two-component relativistic extension of the time-dependent EOM-CC (TD-EOM-CC) approach outlined in refs 39 and 25 that is suitable for computing zero-field splitting in linear absorption spectra. Scalar and spin−orbit relativistic effects are included variationally through the exact-two-component (X2C) transformation scheme,[40−54] which requires the machinery underlying TD-EOM-CC to be generalized to handle two-component (i.e., spin-broken) quantities. We then apply relativistic X2C-TD-EOM-CC with single and double excitations (EOM-CCSD) to simulate atomic absorption spectra of open-shell (Na, K, Mg^+, and Ca^+) and closed-shell (Na^+, K^+, Mg^{2+}, and Ca^{2+}) species and benchmark the accuracy of the computed splittings against those obtained from experiment.

2. THEORY

2.1. Relativistic Two-Component Reference Wave Function. The relativistic TD-EOM-CCSD method developed in this work utilizes spinor MOs from a relativistic two-component reference. In this section, we present a brief review of the relativistic two-component approach; for a more thorough review on relativistic electronic structure theory, we refer readers to refs 55−57.

In two-component methods, the large and small components of the four-component Dirac equation are decoupled by a unitary transformation $\mathcal{U}$ that block-diagonalizes the four-component Hamiltonian:

$$\mathcal{U}^\dagger \hat{\mathcal{H}} \mathcal{U} = \begin{pmatrix} \mathbb{H}^+ & 0_2 \\ 0_2 & \mathbb{H}^- \end{pmatrix} \tag{1}$$

Because only the electronic solutions are of interest, only the two-component Hamiltonian corresponding to electronic solutions, $\mathbb{H}^+$, needs to be computed. Effectively, the two-component transformation eliminates the need to evaluate the small component by "folding" it into the large component:

$$\mathcal{U}\begin{pmatrix} \psi_L \\ \psi_S \end{pmatrix} = \begin{pmatrix} \tilde{\psi}_L \\ 0 \end{pmatrix} \tag{2}$$

In this work, we use the X2C transformation approach[40−54] in which the decoupling scheme is obtained by solving the one-body four-component Dirac−Hartree−Fock equation. The two-electron term is added as the bare Coulomb operator. The leading error in this one-electron X2C approach arises from the neglect of the transformation of the two-electron Coulomb repulsion operator. To compensate for this error, an empirical correction, known as the Boettger factor, is used to scale the one-electron spin−orbit terms in order to approximately account for the two-electron spin−orbit terms.[58] This approach has been shown to be reasonably accurate in describing spin−orbit splittings of both valence and core electrons.[49,50,52,53,59,60]

In the one-electron X2C framework, the transformation (or "picture change") is independent of the two-electron operator. This simplification gives rise to a major advantage of using an effective one-electron X2C approach in the context of post-SCF methods,[61] which is that the two-component transformation $\mathcal{U}$ becomes invariant with respect to the optimization of cluster amplitudes in the CC formalism. This nice property is due to the fact that, in the one-electron X2C framework, the four- to two-component transformation depends on only the choice of basis set through the one-electron Hamiltonian. In this work, we choose to formulate X2C-CC in the general Kramers unrestricted case. For open-shell systems, this could lead to breaking of the time-reversal symmetry.[62] However, in the light element cases tested here, the time-reversal symmetry is mostly maintained.

2.2. Two-Component Equation-of-Motion Coupled-Cluster. Throughout this section, the labels *i,j,k,l* and *a,b,c,d* refer to MOs that are occupied and empty in the reference configuration, respectively. Note that the nature of the relativistic Hamiltonian requires the CC equations to be formulated with complex arithmetic and generalized (spin-broken) amplitudes. Hence, unless stated otherwise, the following discussion assumes that all quantities are complex-valued and spin-broken. These generalizations increase the storage requirements and the number of floating-point operations, but the formal scalings and convergence properties of the ground-state CC calculation and the evolution of the TD-EOM-CC equations are unchanged.

The ground-state CC wave function is given by

$$|\tilde{\Psi}\rangle = e^{\hat{T}}|\tilde{\Phi}_0\rangle \tag{3}$$

where $|\tilde{\Phi}_0\rangle$ is the X2C-transformed reference wave function and $\hat{T}$ represents the cluster operator, defined at the CC with single and double excitations (CCSD) level as

$$\hat{T} = \sum_{ia} t_i^a \hat{a}_a^\dagger \hat{a}_i + \frac{1}{4}\sum_{ijab} t_{ij}^{ab} \hat{a}_a^\dagger \hat{a}_b^\dagger \hat{a}_j \hat{a}_i \tag{4}$$

Here, the symbols $\hat{a}^\dagger$ and $\hat{a}$ represent creation and annihilation operators of second quantization, respectively. The CCSD de-excitation operator is similarly defined as

$$\hat{\Lambda} = \sum_{ia} \lambda_a^i \hat{a}_i^\dagger \hat{a}_a + \frac{1}{4}\sum_{ijab} \lambda_{ab}^{ij} \hat{a}_i^\dagger \hat{a}_j^\dagger \hat{a}_b \hat{a}_a \tag{5}$$

The t and λ amplitudes in eqs 4 and 5 can be determined using a conventional CCSD algorithm,[63−65] modified for complex arithmetic and spin-broken amplitudes.

At the EOM-CCSD level of theory, the n^{th} electronic state is defined by single and double excitations out of the ground state

DOI: 10.1021/acs.jctc.9b00729
J. Chem. Theory Comput. 2019, 15, 6617−6624

$$\hat{R}_n|\tilde{\Psi}\rangle = \left(r_0 + \sum_{ia} r_i^a \hat{a}_a^\dagger \hat{a}_i + \frac{1}{4}\sum_{ijab} r_{ij}^{ab} \hat{a}_a^\dagger \hat{a}_b^\dagger \hat{a}_j \hat{a}_i\right) e^{\hat{T}}|\tilde{\Phi}_0\rangle \tag{6}$$

Here, the expansion coefficients r_0, r_i^a, and r_{ij}^{ab} comprise right-hand eigenfunctions of the normal-ordered similarity-transformed Hamiltonian

$$\bar{H}_N = e^{-\hat{T}}\hat{H}e^{\hat{T}} - E_{CC} \tag{7}$$

within the space spanned by the reference, singly excited, and doubly excited determinants; these eigenfunctions satisfy

$$\bar{H}_N\hat{R}_n|\tilde{\Phi}_0\rangle = \omega_n\hat{R}_n|\tilde{\Phi}_0\rangle \tag{8}$$

where E_{CC} represents the ground-state energy, and ω_n represents the difference between the energy of the n^{th} excited state and that of the ground state. Because the similarity-transformed Hamiltonian is non-Hermitian, a set of left-hand eigenfunctions satisfying

$$\langle\tilde{\Phi}_0|\hat{L}_n\bar{H}_N = \langle\tilde{\Phi}_0|\hat{L}_n\omega_n \tag{9}$$

similarly defines the left-hand excited-state wave functions

$$\langle\tilde{\Phi}_0|e^{-\hat{T}}\hat{L}_n = \langle\tilde{\Phi}_0|e^{-\hat{T}}\left(l_0 + \sum_{ia} l_a^i \hat{a}_i^\dagger \hat{a}_a + \frac{1}{4}\sum_{ijab} l_{ab}^{ij} \hat{a}_i^\dagger \hat{a}_j^\dagger \hat{a}_b \hat{a}_a\right) \tag{10}$$

The right- and left-hand wave functions for the ground state are recovered by specifying $\hat{R}_0 = 1$ and $\hat{L}_0 = 1 + \hat{\Lambda}$, respectively, and $l_0 = 0$ for all excited states.

2.3. Moment-Based Determination of Linear Absorption Spectra. Linear absorption spectra can be generated from a time-domain simulation in which one propagates the right- and left-hand CC wave functions in the presence of an oscillating electric field (for resonant or near-resonant spectra) or a delta pulse (for broad-band spectra). The time-dependent dipole moment then carries information regarding the excited states that are accessed via the external perturbation. In the present formalism, however, a time-dependent external electric field is not added to the Hamiltonian directly. Rather, the absorption line shape is extracted from the Fourier transform of the dipole autocorrelation function.

The working equations of the present approach can be obtained in the following manner,[39,66,67] beginning with the Fermi's Golden Rule expression for the ξ-component of the isotropic linear absorption line shape

$$I_\xi(\omega) = \sum_{IF} \rho_I |\langle\Psi_I|\hat{\mu}_\xi|\Psi_F\rangle|^2 \delta(E_F - E_I - \omega) \tag{11}$$

Here, ω is the frequency of the incident light, the sums run over all initial and final states, Ψ_I and Ψ_F, respectively, ρ_I represents the Boltzmann factor for the initial state, Ψ_I, and $\hat{\mu}_\xi$ is the component of the dipole operator that is parallel to the ξ axis ($\xi \in x,y,z$). Because at 0 K the Boltzmann factor is zero for all excited states, we consider only the sum over final states

$$I_\xi(\omega) = \sum_F |\langle\Psi_0|\hat{\mu}_\xi|\Psi_F\rangle|^2 \delta(\omega_F - \omega) \tag{12}$$

Substituting in the ground and excited states from EOM-CC and replacing the Dirac δ with its Fourier integral, $\delta(\omega') = \int_{-\infty}^{\infty} dt\ e^{iw't}$, we obtain

$$I_\xi(\omega) = \int_{-\infty}^{\infty} dt\ e^{-iwt} \sum_F \langle\tilde{\Phi}_0|\hat{L}_0\bar{\mu}_\xi\hat{R}_F|\tilde{\Phi}_0\rangle\langle\tilde{\Phi}_0|\hat{L}_F e^{i\omega_F t}\bar{\mu}_\xi\hat{R}_0|\tilde{\Phi}_0\rangle \tag{13}$$

where $\bar{\mu}_\xi$ represents the ξth component of the similarity-transformed dipole operator

$$\bar{\mu}_\xi = e^{-\hat{T}}\hat{\mu}_\xi e^{\hat{T}} \tag{14}$$

Because $\langle\tilde{\Phi}_0|\hat{L}_F$ is an eigenfunction of $\bar{H}_N$, we can replace $e^{i\omega_F t}$ with $e^{i\bar{H}_N t}$ and then use the closure relation, $\sum_P \hat{R}_P|\tilde{\Phi}_0\rangle\langle\tilde{\Phi}_0|\hat{L}_P = \hat{1}$, to achieve

$$I_\xi(\omega) = \int_{-\infty}^{\infty} dt\ e^{-iwt}\langle\tilde{\Phi}_0|\hat{L}_0\bar{\mu}_\xi e^{i\bar{H}_N t}\bar{\mu}_\xi\hat{R}_0|\tilde{\Phi}_0\rangle \tag{15}$$

Left and right dipole functions can be defined such that

$$I_\xi(\omega) = \int_{-\infty}^{\infty} dt\ e^{-iwt}\langle\tilde{M}_\xi(t)|M_\xi(0)\rangle \tag{16}$$

or

$$I_\xi(\omega) = \int_{-\infty}^{\infty} dt\ e^{-iwt}\langle\tilde{M}_\xi(0)|M_\xi(-t)\rangle \tag{17}$$

At the TD-EOM-CCSD level of theory, these functions are expanded linearly as

$$\langle\tilde{M}_\xi(t)| = \langle\tilde{\Phi}_0|\left(\tilde{m}_0 + \sum_{ia}\tilde{m}_a^i\hat{a}_i^\dagger\hat{a}_a + \frac{1}{4}\sum_{ijab}\tilde{m}_{ab}^{ij}\hat{a}_i^\dagger\hat{a}_j^\dagger\hat{a}_b\hat{a}_a\right) \tag{18}$$

and

$$|M_\xi(t)\rangle = \left(m_0 + \sum_{ia} m_i^a\hat{a}_a^\dagger\hat{a}_i + \frac{1}{4}\sum_{ijab} m_{ij}^{ab}\hat{a}_a^\dagger\hat{a}_b^\dagger\hat{a}_j\hat{a}_i\right)|\tilde{\Phi}_0\rangle \tag{19}$$

and the $\tilde{m}$ and m amplitudes are defined at time $t = 0$ by

$$\langle\tilde{M}_\xi(0)| = \langle\tilde{\Phi}_0|(1 + \hat{\Lambda})\bar{\mu}_\xi \tag{20}$$

and

$$|M_\xi(0)\rangle = \bar{\mu}_\xi|\tilde{\Phi}_0\rangle \tag{21}$$

respectively. The m and $\tilde{m}$ amplitudes can be evolved in time according to the Schrödinger equation

$$\frac{\partial}{\partial t}|M_\xi(t)\rangle = -i\bar{H}_N|M_\xi(t)\rangle \tag{22}$$

and its complex conjugate

$$\frac{\partial}{\partial t}\langle M_\xi(t)| = i\langle M_\xi(t)|\bar{H}_N \tag{23}$$

respectively. It is important to note that eqs 16 and 17 yield equivalent line shapes; therefore, an absorption spectrum can be obtained by propagating either the left or the right dipole function, meaning that either the m or $\tilde{m}$ amplitudes need to be evolved in time but not both.[39] This result contrasts with standard EOM-CC theory, in which both left and right eigenvalue problems must be solved in order to determine oscillator strengths.

DOI: 10.1021/acs.jctc.9b00729
J. Chem. Theory Comput. 2019, 15, 6617−6624

3. RESULTS AND DISCUSSION

The real-time propagation of the relativistic X2C-TD-EOM-CCSD moment function is implemented in the Chronus Quantum software package.[68] In the current implementation, the evaluation of the matrix−vector products (i.e., the construction of sigma vectors) is powered by the TiledArray[69] library. All computations employed the 6-31G basis set,[70−72] unless otherwise noted. It has been shown that the time evolution of the left and right dipole functions gives rise to nearly identical spectroscopic observables.[39] Therefore, we choose to obtain the time signals by propagating the right dipole function only (eq 17), which is done using a fourth-order Runge−Kutta (RK4) numerical integrator. For these calculations, a step size of either 0.24 or 0.024 attoseconds is used and propagated for around 12 fs or until the spectrum is converged. The Padé transform of the dipole autocorrelation function is used to resolve the linear absorption spectra.[25,50,60,73] Prior to the transformation into the frequency domain, the signal is damped using the function $e^{-(1/2)\Gamma t}$, where t is time and Γ is the full width at half maximum (fwhm). For these calculations, a damping constant of 0.00002 au was used.

3.1. Sodium D-Lines: Relativistic vs Nonrelativistic. The lowest-energy excitation of a sodium atom corresponds to the $^2S \rightarrow {}^2P$ electronic transition. Due to spin−orbit coupling, the six-fold degenerate ^2P term splits into $^2P_{1/2}$ and $^2P_{3/2}$ levels, giving rise to a bright doublet known as the sodium D-lines ($^2S_{1/2} \rightarrow {}^2P_{1/2}$ and $^2S_{1/2} \rightarrow {}^2P_{3/2}$). Splitting between sodium D-lines is experimentally measured to be 2.1 meV,[74] which can be captured only with an accurate relativistic electronic structure method.

The time evolution of the dipole autocorrelation function of a sodium atom is show in Figure 1A. This series is obtained by propagating the dipole autocorrelation function forward in time, resulting in the complex-valued oscillating dipole function. This dipole function can be transformed from the time domain into the frequency domain, resulting in the absorption spectra seen in Figure 1B.

Atomic absorption spectra computed using relativistic and nonrelativistic TD-EOM-CCSD are compared in Figure 1B. In the two-component TD-EOM-CCSD formalism developed here, relativistic corrections, such as the scalar relativity and spin−orbit coupling, come from the variational reference wave function. The nonrelativistic TD-EOM-CCSD uses a two-component reference wave function without any relativistic correction or transformation, also known as complex generalized Hartree−Fock (ℂ-GHF).[75] When using ℂ-GHF as the reference wave function, the resulting spectrum has a single peak for the $^2S \rightarrow {}^2P$ transition. In contrast, when a relativistic X2C reference is used, the splitting between the $^2P_{1/2}$ and $^2P_{3/2}$ states is clearly seen with an estimated splitting of ∼2.0 meV. While the peak positions appear slightly red-shifted (by ∼0.1 eV) compared to experimental values,[74] the error in the zero-field splitting is only ∼0.1 meV.

The relativistic X2C-TD-EOM-CCSD also correctly predicts the relative oscillator strength between the $^2S_{1/2} \rightarrow {}^2P_{1/2}$ and $^2S_{1/2} \rightarrow {}^2P_{3/2}$ transitions. Although Kramers unrestricted reference is used for open-shell atoms, Kramers symmetry is largely maintained in the ground-state X2C-HF reference for light atoms studied here, and the $^2P_{1/2}$ and $^2P_{3/2}$ states are

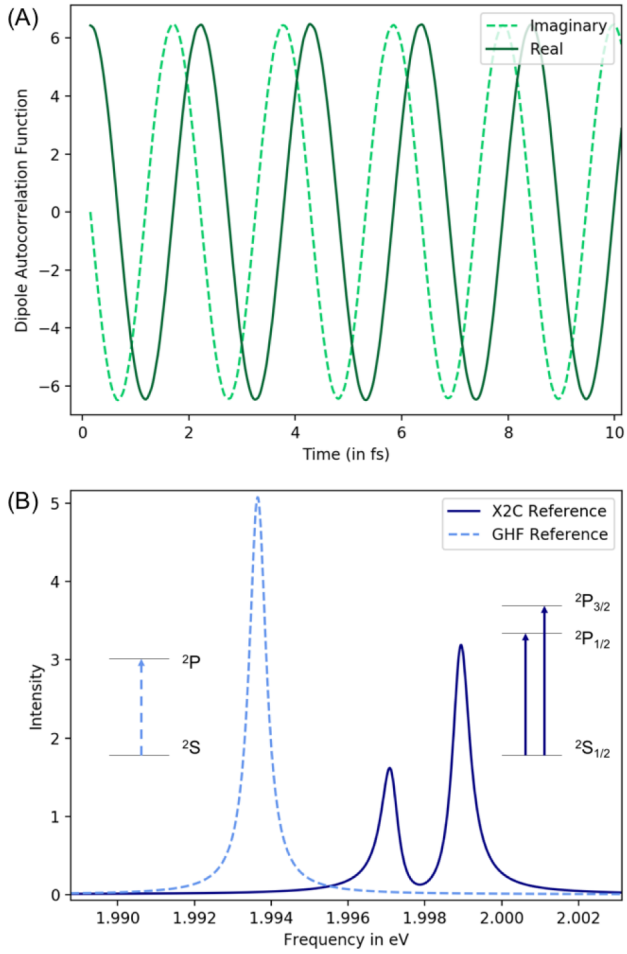

Figure 1. (A) Time propagation of both the real and imaginary parts of the dipole autocorrelation function. (B) Absorption spectra from TD-EOM-CCSD of a sodium atom using both the nonrelativistic ℂ-GHF reference and the relativistic X2C reference wave functions. Absorption spectra were obtained through Padé transformation of the dipole time signal into the frequency domain.

two- and four-fold degenerate, respectively. As a result, the $^2S_{1/2} \rightarrow {}^2P_{3/2}$ peak is almost twice as intense as the $^2S_{1/2} \rightarrow {}^2P_{3/2}$ transition. In contrast, because all six $^2S \rightarrow {}^2P$ transitions are degenerate in the nonrelativistic limit, the height of the peak with the ℂ-GHF reference is the sum of the heights of the two peaks from the simulations with the X2C reference.

3.2. Zero-Field Splitting of S → P Photoabsorption Spectra. To further analyze the quality of relativistic X2C-TD-EOM-CCSD, S → P excitations in a series of alkali metal atoms and alkaline earth metal cations are computed. In Table 1, the excited-state zero-field splitting of the calculated atomic spectra is compared to experiments. For open-shell atoms (Na, K, Mg^+, Ca^+) with a single valence electron, the computed peaks correspond to $^2S_{1/2} \rightarrow {}^2P_{1/2}$ and $^2S_{1/2} \rightarrow {}^2P_{3/2}$.

Table 1 shows that the computed $^2S_{1/2} \rightarrow {}^2P_{1/2}$ and $^2S_{1/2} \rightarrow {}^2P_{3/2}$ peaks are slightly red-shifted by less than 0.2 eV for neutral atoms compared to experiments. This is likely due to the small size of the basis set used in these calculations. The error in peak position decreases for atomic cations. The extra nuclear charge in cationic species gives rise to a higher degree of contraction of the electron wave function. As a result, a

DOI: 10.1021/acs.jctc.9b00729
J. Chem. Theory Comput. 2019, 15, 6617−6624

Table 1. Zero-Field Splitting of Atomic Absorption Spectra (in eV) for the $^2S_{1/2} \rightarrow {}^2P_{1/2}$ and $^2S_{1/2} \rightarrow {}^2P_{3/2}$ Transitions of Open-Shell Alkali Metal Atoms and Alkaline Earth Cations, Computed at the X2C-TD-EOM-CCSD/6-31G Level of Theory and Compared with Experimental Values[74]

	Na	Mg^+	K	Ca^+
X2C-TD-EOM-CCSD				
$^2S_{1/2} \rightarrow {}^2P_{1/2}$	1.9970	4.2831	1.4286	3.1035
$^2S_{1/2} \rightarrow {}^2P_{3/2}$	1.9989	4.2926	1.4334	3.1252
splitting	0.0019	0.0095	0.0048	0.0218
Experiment				
$^2S_{1/2} \rightarrow {}^2P_{1/2}$	2.1023	4.4224	1.6100	3.1233
$^2S_{1/2} \rightarrow {}^2P_{3/2}$	2.1044	4.4338	1.6171	3.1510
splitting	0.0021	0.0114	0.0071	0.0277

smaller basis set is better able to describe electronic transitions in atomic cations than that in corresponding neutral atoms.

The computed zero-field splittings of the absorption peaks are in excellent agreement with experiments, with the largest error of 5.9 meV for the Ca^+ test case. As expected, the zero-field splitting within the alkali group of atoms and the alkaline earth metal cations increases with increasing principal quantum number of the valence electron. Orbital contraction and increased nuclear charge in atomic cations lead to a larger spin−orbit coupling. As a result, among isoelectronic atoms (e.g., Na and Mg^+), cations have a larger zero-field splitting than isoelectronic neutral atoms.

3.3. Photoabsorption of Spin-Forbidden Transitions.

For closed-shell systems, such as Na^+, K^+, Mg^{2+}, and Ca^{2+}, the lowest-energy excitation in nonrelativistic calculations, such as those using the ℂ-GHF reference, is the spin-allowed $^1S \rightarrow {}^1P$ transition. In the relativistic X2C-TD-EOM-CC calculations, an additional lower-energy peak appears in this spectral region (Figure 2). The $^1S_0 \rightarrow {}^3P_1$ transition becomes dipole-allowed due to the spin−orbit coupling but has a smaller intensity than the spin-allowed $^1S_0 \rightarrow {}^1P_1$ transition.

Table 2 compares computed peak positions using different basis sets with those optioned from experimentally obtained values. All computed peaks using a smaller 6-31G basis are blue-shifted by 1−2 eV compared to the experiments. For isoelectronic closed-shell ions (e.g., K^+ and Ca^{2+}), 2+ cations have a larger zero-field splitting, in agreement with experiment.

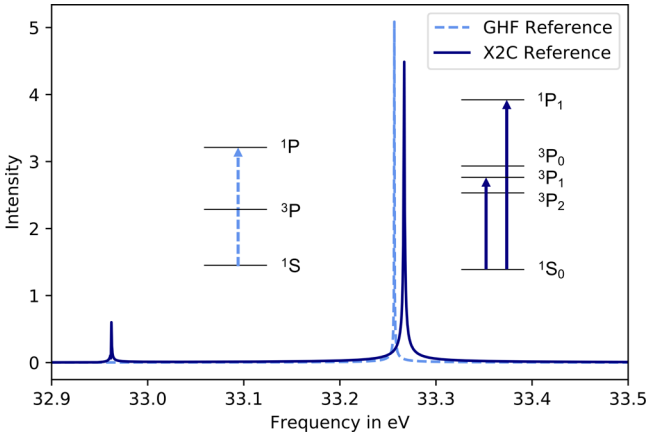

Figure 2. Absorption spectra from TD-EOM-CCSD/Sapporo-DZP-2012-ALL of a Na^+ using both the nonrelativistic ℂ-GHF reference and the relativistic X2C reference wave functions.

Table 2. X2C-TD-EOM-CCSD-Computed Atomic Absorption Spectra (in eV) for the $^1S_0 \rightarrow {}^3P_1$ and $^1S_0 \rightarrow {}^1P_1$ Transitions in Closed-Shell Noble Gas-Like Cations, Compared with Experimental Values[74] along with Mean Absolute Errors (MAEs) in Peak Position

	Na^+	Mg^{2+}	K^+	Ca^{2+}
6-31G				
$^1S_0 \rightarrow {}^3P_1$	35.1108	54.8683	21.2317	31.0904
$^1S_0 \rightarrow {}^1P_1$	35.3054	55.2221	21.4773	31.4645
splitting	0.1946	0.3538	0.2456	0.3741
MAE	1.4061			
Sapporo-DZP-2012-ALL				
$^1S_0 \rightarrow {}^3P_1$	32.9622	53.0249	20.2357	30.2354
$^1S_0 \rightarrow {}^1P_1$	33.2667	53.5256	20.5704	30.6781
splitting	0.3045	0.5007	0.3347	0.4427
MAE	0.0387			
Experiment				
$^1S_0 \rightarrow {}^3P_1$	32.9413	52.9249	20.2382	30.2435
$^1S_0 \rightarrow {}^1P_1$	33.3224	53.5029	20.6381	30.7104
splitting	0.3811	0.5780	0.3999	0.4669

This is due to an increased spin−orbit coupling arising from increased nuclear charge and contraction of orbitals. Calculations using the 6-31G basis set significantly overestimate the absorption peak positions by 1−2 eV, with a larger error for smaller cations. In contrast to systems in the previous section, electronic transitions in these closed-shell atoms involve core-electron excitations. The poor description of core-electron wave functions using the 6-31G basis set leads to an overcontracted core-electron wave function and significantly blue-shifted spectra. Increasing the size of the basis set and flexibility of core orbitals with the relativistic Sapporo-DZP-2012-ALL basis,[76] the accuracy of computed spectra is drastically improved, with <0.04 eV in mean absolute error in peak position and <0.08 eV error in peak splitting.

For comparison, relativistic time-dependent density functional theory (X2C-TDDFT) calculations[52,77] (Table 3) were

Table 3. X2C-TDDFT-Computed Atomic Absorption Spectra (in eV) for the $^1S_0 \rightarrow {}^3P_1$ and $^1S_0 \rightarrow {}^1P_1$ Transitions in Closed-Shell Noble Gas-Like Cations, Compared with Experimental Values[74] along with Mean Absolute Errors (MAE) in Peak Position[a]

	Na^+	Mg^{2+}	K^+	Ca^{2+}
TD-X2C-B3LYP				
$^1S_0 \rightarrow {}^3P_1$	30.1930	49.4285	19.6621	28.7842
$^1S_0 \rightarrow {}^1P_1$	30.5015	49.9755	19.8995	29.2494
splitting	0.3086	0.5470	0.2375	0.4651
MAE	2.2521			
TD-X2C-BP86				
$^1S_0 \rightarrow {}^3P_1$	29.2987	48.8303	18.8295	28.7896
$^1S_0 \rightarrow {}^1P_1$	29.5308	49.2456	19.1039	29.2005
splitting	0.2321	0.4153	0.2744	0.4109
MAE	2.7116			
TD-X2C-BHandH				
$^1S_0 \rightarrow {}^3P_1$	31.9982	51.3506	19.8055	29.5461
$^1S_0 \rightarrow {}^1P_1$	32.3611	51.9756	20.1467	30.0574
splitting	0.3629	0.6250	0.3412	0.5113
MAE	0.9101			

[a]Sapporo-DZP-2012-ALL is used for all calculations.

DOI: 10.1021/acs.jctc.9b00729
J. Chem. Theory Comput. 2019, 15, 6617−6624

performed using the Sapporo-DZP-2012-ALL basis with the B3LYP, BP86, and BHandH functionals. Looking at the absolute peak positions, the X2C-TDDFT results are always red-shifted, with errors between ∼0.5 and 4.5 eV. For all results analyzed here, X2C-TD-EOM-CCSD outperforms X2C-TDDFT.

4. CONCLUSIONS

Here, we have discussed an implementation of relativistic X2C-TD-EOM-CCSD. By using X2C as our reference wave function and expanding the machinery of TD-EOM-CCSD to handle two-component calculations, we are able to observe relativistic effects in the calculated absorption spectra. The approach was validated by considering the zero-field splitting in Na, Mg^+, K, and Ca^+ and the appearance of spin-forbidden transitions in Na^+, Mg^{2+}, K^+, and Ca^{2+}. By comparing these calculations to similar TD-EOM-CCSD calculations with a nonrelativistic reference, we can clearly see the splitting of peaks occurring in the open-shell species and the appearance of previously dark transitions in the closed-shell species. Compared to spectra obtained by X2C-TDDFT, X2C-TD-EOM-CCSD results are consistently in better agreement with experiment.

The primary advantage of working in the time domain is a drastic reduction in the storage requirements of the approach, as compared to those of a standard, frequency-domain implementation of EOM-CCSD (or X2C-EOM-CCSD). For example, a conventional EOM-CCSD calculation of an absorption spectra involving N excited states requires the storage of N copies of right-hand and left-hand EOM-CCSD wave functions, as well as several times as many comparably sized objects during the actual diagonalization of $\bar{H}_N$ (i.e., additional subspace vectors and sigma vectors). On the other hand, TD-EOM-CCSD requires only the storage of a single copy of the left-hand and right-hand dipole moment functions and a small number of comparably sized objects to perform the time integration (in this case, according to the RK4 scheme). Further, while other time-dependent formulations of EOM-CCSD require propagation of both the left and right wave functions, the moment-based formalism requires only the propagation of either the left or right dipole function, effectively decreasing the required number of floating-point operations by a factor of 2. This reduction is important as time-domain calculations generally involve far more floating-point operations than are required by frequency-domain approaches (note, however, that the formal scalings of TD-EOM-CC and EOM-CC are the same; only the prefactor increases in the time-dependent case). This implementation of X2C-TD-EOM-CCSD sets the groundwork for simulations of electron dynamics in the presence of time-varying electromagnetic fields, so that nonequilibrium dynamics with a variational treatment of relativistic effects can be considered in the future.

AUTHOR INFORMATION

Corresponding Authors

*E-mail: deprince@chem.fsu.edu.
*E-mail: xsli@uw.edu.

ORCID

David B. Williams-Young: 0000-0003-2735-3706
Daniel R. Nascimento: 0000-0002-2126-8378
A. Eugene DePrince, III: 0000-0003-1061-2521
Xiaosong Li: 0000-0001-7341-6240

Funding

This work was supported by the U.S. Department of Energy, Office of Science, Basic Energy Sciences, under Award LAB 17-1775, as part of the Computational Chemical Sciences Program. L.K. is thankful for the fellowship support from the MolSSI software institute. The development of the two-component method was funded by the U.S. Department of Energy (DE-SC0006863). The development of the Chronus Quantum open source software package is supported by the National Science Foundation (OAC-1663636). Computations were facilitated through the use of advanced computational, storage, and networking infrastructure provided by the Hyak supercomputer system at the University of Washington, funded by the Student Technology Fee and the National Science Foundation (MRI-1624430).

Notes

The authors declare no competing financial interest.

REFERENCES

(1) Pyykkö, P. Relativistic Effects in Structural Chemistry. *Chem. Rev.* **1988**, *88*, 563−594.
(2) Pyykkö, P. Relativistic Effects in Chemistry: More Common Than You Thought. *Annu. Rev. Phys. Chem.* **2012**, *63*, 45−64.
(3) Marian, C. M. Spin-Orbit Coupling and Intersystem Crossing in Molecules. *WIREs Comput. Mol. Sci.* **2012**, *2*, 187−203.
(4) Shavitt, I.; Bartlett, R. J. *Many -Body Methods in Chemistry and Physics; MBPT and Coupled-Cluster Theory*; Cambridge University Press, 2009.
(5) Monkhorst, H. J. Calculation of Properties With the Coupled-cluster Method. *Int. J. Quantum Chem.* **1977**, *12*, 421−432.
(6) Koch, H.; Jørgensen, P. Coupled Cluster Response Functions. *J. Chem. Phys.* **1990**, *93*, 3333−3344.
(7) Mukherjee, D.; Mukherjee, P. A response-function approach to the direct calculation of the transition-energy in a multiple-cluster expansion formalism. *Chem. Phys.* **1979**, *39*, 325−335.
(8) Emrich, K. An extension of the coupled cluster formalism to excited states (I). *Nucl. Phys. A* **1981**, *351*, 379−396.
(9) Stanton, J. F.; Bartlett, R. J. The Equation of Motion Coupled-Cluster Method. A Systematic Biorthogonal Approach to Molecular Excitation Energies, Transition Probabilities, and Excited State Properties. *J. Chem. Phys.* **1993**, *98*, 7029−7039.
(10) Helgaker, T.; Coriani, S.; Jørgensen, P.; Kristensen, K.; Olsen, J.; Ruud, K. Recent advances in wave function-based methods of molecular-property calculations. *Chem. Rev.* **2012**, *112*, 543−631.
(11) Peng, B.; Lestrange, P. J.; Goings, J. J.; Caricato, M.; Li, X. Energy-Specific Equation-of-Motion Coupled-Cluster Methods for High-Energy Excited States: Application to K-Edge X-Ray Absorption Spectroscopy. *J. Chem. Theory Comput.* **2015**, *11*, 4146−4153.
(12) Cheng, L.; Wang, F.; Stanton, J. F.; Gauss, J. Perturbative Treatment of Spin-orbit-coupling within Spin-free Exact Two-component Theory using Equation-of-motion Coupled-cluster Methods. *J. Chem. Phys.* **2018**, *148*, 044108.
(13) Epifanovsky, E.; Klein, K.; Stopkowicz, S.; Gauss, J.; Krylov, A. I. Spin-orbit couplings within the equation-of-motion coupled-cluster framework: Theory, implementation, and benchmark calculations. *J. Chem. Phys.* **2015**, *143*, 064102.
(14) Klein, K.; Gauss, J. Perturbative Calculation of Spin-orbit Splittings using the Equation-of-motion Ionization-potential Coupled-cluster Ansatz. *J. Chem. Phys.* **2008**, *129*, 194106.
(15) Christiansen, O.; Gauss, J.; Schimmelpfennig, B. Spin-orbit Coupling Constants from Coupled-cluster Response Theory. *Phys. Chem. Chem. Phys.* **2000**, *2*, 965−971.
(16) Cao, Z.; Li, Z.; Wang, F.; Liu, W. Combining the spin-separated exact two-component relativistic Hamiltonian with the equation-of-motion coupled-cluster method for the treatment of spinorbit

DOI: 10.1021/acs.jctc.9b00729
J. Chem. Theory Comput. 2019, 15, 6617−6624

splittings of light and heavy elements. *Phys. Chem. Chem. Phys.* **2017**, *19*, 3713−3721.
(17) Yang, D.-D.; Wang, F.; Guo, J. Equation of Motion Coupled Cluster Method for Electron Attached States with Spin-orbit Coupling. *Chem. Phys. Lett.* **2012**, *531*, 236−241.
(18) Tu, Z.; Wang, F.; Li, X. Equation-of-motion Coupled-Cluster Method for Ionized States with Spin-orbit Coupling. *J. Chem. Phys.* **2012**, *136*, 174102.
(19) Wang, Z.; Tu, Z.; Wang, F. Equation-of-Motion Coupled-Cluster Theory for Excitation Energies of Closed-Shell Systems with SpinOrbit Coupling. *J. Chem. Theory Comput.* **2014**, *10*, 5567−5576.
(20) Asthana, A.; Liu, J.; Cheng, L. Exact two-component equation-of-motion coupled-cluster singles and doubles method using atomic mean-field spin-orbit integrals. *J. Chem. Phys.* **2019**, *150*, 074102.
(21) Shee, A.; Saue, T.; Visscher, L.; Severo Pereira Gomes, A. Equation-of-motion Coupled-cluster Theory based on the 4-component Dirac-Coulomb(-Gaunt) Hamiltonian. Energies for Single Electron Detachment, Attachment, and Electronically Excited States. *J. Chem. Phys.* **2018**, *149*, 174113.
(22) Akinaga, Y.; Nakajima, T. Two-Component Relativistic Equation-of-Motion Coupled-Cluster Methods for Excitation Energies and Ionization Potentials of Atoms and Molecules. *J. Phys. Chem. A* **2017**, *121*, 827−835.
(23) Liu, J.; Cheng, L. An Atomic Mean-field Spin-orbit Approach within Exact Two-component Theory for a Non-perturbative Treatment of Spin-orbit Coupling. *J. Chem. Phys.* **2018**, *148*, 144108.
(24) Pathak, H.; Sasmal, S.; Nayak, M. K.; Vaval, N.; Pal, S. Relativistic Equation-of-motion Coupled-cluster Method for the Electron Attachment Problem. *Comput. Theor. Chem.* **2016**, *1076*, 94−100.
(25) Nascimento, D. R.; DePrince, A. E. Simulation of Near-Edge X-ray Absorption Fine Structure with Time-Dependent Equation-of-Motion Coupled-Cluster Theory. *J. Phys. Chem. Lett.* **2017**, *8*, 2951−2957.
(26) Tussupbayev, S.; Govind, N.; Lopata, K.; Cramer, C. J. Comparison of Real-time and Linear-response Time-dependent Density Functional Theories for Molecular Chromophores Ranging from Sparse to High Densities of States. *J. Chem. Theory Comput.* **2015**, *11*, 1102−1109.
(27) Goings, J. J.; Lestrange, P. J.; Li, X. Real-Time Time-Dependent Electronic Structure Theory. *WIREs Comput. Mol. Sci.* **2018**, *8*, No. e1341.
(28) Schönhammer, K.; Gunnarsson, O. Time-dependent approach to the calculation of spectral functions. *Phys. Rev. B: Condens. Matter Mater. Phys.* **1978**, *18*, 6606−6614.
(29) Huber, C.; Klamroth, T. Explicitly Time-dependent Coupled Cluster Singles Doubles Calculations of Laser-driven Many-electron Dynamics. *J. Chem. Phys.* **2011**, *134*, 054113.
(30) Kvaal, S. Ab initio quantum dynamics using coupled-cluster. *J. Chem. Phys.* **2012**, *136*, 194109.
(31) Sato, T.; Pathak, H.; Orimo, Y.; Ishikawa, K. L. Communication: Time-dependent optimized coupled-cluster method for multielectron dynamics. *J. Chem. Phys.* **2018**, *148*, 051101.
(32) Pedersen, T. B.; Kvaal, S. Symplectic integration and physical interpretation of time-dependent coupled-cluster theory. *J. Chem. Phys.* **2019**, *150*, 144106.
(33) Sonk, J. A.; Caricato, M.; Schlegel, H. B. TD-CI Simulation of the Electronic Optical Response of Molecules in Intense Fields: Comparison of RPA, CIS, CIS(D), and EOM-CCSD. *J. Phys. Chem. A* **2011**, *115*, 4678−4690.
(34) Luppi, E.; Head-Gordon, M. Computation of High-harmonic Generation Spectra of H_2 and N_2 in Intense Laser Pulses using Quantum Chemistry Methods and Time-dependent Density Functional Theory. *Mol. Phys.* **2012**, *110*, 909−923.
(35) Hoodbhoy, P.; Negele, J. W. Time-dependent coupled-cluster approximation to nuclear dynamics. I. Application to a solvable model. *Phys. Rev. C: Nucl. Phys.* **1978**, *18*, 2380−2394.
(36) Hoodbhoy, P.; Negele, J. W. Time-dependent coupled-cluster approximation to nuclear dynamics. II. General formulation. *Phys. Rev. C: Nucl. Phys.* **1979**, *19*, 1971.
(37) Pawlowski, F.; Olsen, J.; Jørgensen, P. Molecular response properties from a Hermitian eigenvalue equation for a time-periodic Hamiltonian. *J. Chem. Phys.* **2015**, *142*, 114109.
(38) Coriani, S.; Pawlowski, F.; Olsen, J.; Jørgensen, P. Molecular response properties in equation of motion coupled cluster theory: A time-dependent perspective. *J. Chem. Phys.* **2016**, *144*, 024102.
(39) Nascimento, D. R.; DePrince, A. E. Linear Absorption Spectra from Explicitly Time-Dependent Equation-of-Motion Coupled-Cluster Theory. *J. Chem. Theory Comput.* **2016**, *12*, 5834−5840.
(40) Kutzelnigg, W.; Liu, W. Quasirelativistic Theory Equivalent to Fully Relativistic Theory. *J. Chem. Phys.* **2005**, *123*, 241102.
(41) Liu, W.; Peng, D. Infinite-Order Quasirelativistic Density Functional Method Based on the Exact Matrix Quasirelativistic Theory. *J. Chem. Phys.* **2006**, *125*, 044102.
(42) Peng, D.; Liu, W.; Xiao, Y.; Cheng, L. Making Four- and Two-Component Relativistic Density Functional Methods Fully Equivalent Based on the Idea of From Atoms to Molecule. *J. Chem. Phys.* **2007**, *127*, 104106.
(43) Ilias, M.; Saue, T. An Infinite-Order Relativistic Hamiltonian by a Simple One-Step Transformation. *J. Chem. Phys.* **2007**, *126*, 064102.
(44) Liu, W.; Peng, D. Exact Two-component Hamiltonians Revisited. *J. Chem. Phys.* **2009**, *131*, 031104.
(45) Liu, W. Ideas of Relativistic Quantum Chemistry. *Mol. Phys.* **2010**, *108*, 1679−1706.
(46) Saue, T. Relativistic Hamiltonians for Chemistry: A Primer. *ChemPhysChem* **2011**, *12*, 3077−3094.
(47) Li, Z.; Xiao, Y.; Liu, W. On the Spin Separation of Algebraic Two-Component Relativistic Hamiltonians. *J. Chem. Phys.* **2012**, *137*, 154114.
(48) Peng, D.; Middendorf, N.; Weigend, F.; Reiher, M. An Efficient Implementation of Two-Component Relativistic Exact-Decoupling Methods for Large Molecules. *J. Chem. Phys.* **2013**, *138*, 184105.
(49) Egidi, F.; Goings, J. J.; Frisch, M. J.; Li, X. Direct Atomic-Orbital-Based Relativistic Two-Component Linear Response Method for Calculating Excited-State Fine Structures. *J. Chem. Theory Comput.* **2016**, *12*, 3711−3718.
(50) Goings, J. J.; Kasper, J. M.; Egidi, F.; Sun, S.; Li, X. Real Time Propagation of the Exact Two Component Time-Dependent Density Functional Theory. *J. Chem. Phys.* **2016**, *145*, 104107.
(51) Konecny, L.; Kadek, M.; Komorovsky, S.; Malkina, O. L.; Ruud, K.; Repisky, M. Acceleration of Relativistic Electron Dynamics by Means of X2C Transformation: Application to the Calculation of Nonlinear Optical Properties. *J. Chem. Theory Comput.* **2016**, *12*, 5823−5833.
(52) Egidi, F.; Sun, S.; Goings, J. J.; Scalmani, G.; Frisch, M. J.; Li, X. Two-Component Non-Collinear Time-Dependent Spin Density Functional Theory for Excited State Calculations. *J. Chem. Theory Comput.* **2017**, *13*, 2591−2603.
(53) Petrone, A.; Williams-Young, D. B.; Sun, S.; Stetina, T. F.; Li, X. An Efficient Implementation of Two-Component Relativistic Density Functional Theory with Torque-Free Auxiliary Variables. *Eur. Phys. J. B* **2018**, *91*, 169.
(54) Liu, W.; Xiao, Y. Relativistic Time-dependent Density Functional Theories. *Chem. Soc. Rev.* **2018**, *47*, 4481−4509.
(55) Dyall, K. G.; Fægri, K., Jr. *Introduction to Relativistic Quantum Chemistry*; Oxford University Press, 2007.
(56) Reiher, M.; Wolf, A. *Relativistic Quantum Chemistry*, 2nd ed.; Wiley-VCH, 2015.
(57) Liu, W. *Handbook of Relativistic Quantum Chemistry*; Springer-Verlag: Berlin Heidelberg, 2017.
(58) Boettger, J. C. Approximate Two-Electron Spin-Orbit Coupling Term For Density-Functional-Theory DFT Calculations Using The Douglas-Kroll-Hess Transformation. *Phys. Rev. B: Condens. Matter Mater. Phys.* **2000**, *62*, 7809−7815.

DOI: 10.1021/acs.jctc.9b00729
J. Chem. Theory Comput. 2019, 15, 6617−6624

(59) Williams-Young, D.; Egidi, F.; Li, X. Relativistic Two-Component Particle-Particle Tamm-Dancoff Approximation. *J. Chem. Theory Comput.* **2016**, *12*, 5379−5384.
(60) Kasper, J. M.; Lestrange, P. J.; Stetina, T. F.; Li, X. Modeling $L_{2,3}$-Edge X-ray Absorption Spectroscopy with Real-Time Exact Two-Component Relativistic Time-Dependent Density Functional Theory. *J. Chem. Theory Comput.* **2018**, *14*, 1998−2006.
(61) Jenkins, A. J.; Liu, H.; Kasper, J. M.; Frisch, M. J.; Li, X. Variational Relativistic Complete Active Space Self-Consistent Field Method. *J. Chem. Theory Comput.* **2019**, *15*, 2974−2982.
(62) Lestrange, P. J.; Williams-Young, D. B.; Petrone, A.; Jimenez-Hoyos, C. A.; Li, X. An Efficient Implementation of Variation After Projection Generalized Hartree-Fock. *J. Chem. Theory Comput.* **2018**, *14*, 588−596.
(63) Crawford, D. T.; Schaefer, H. F., III *Rev. Comp Chem.* **2007**, *14*, 33−136.
(64) Stanton, J. F.; Gauss, J.; Watts, J. D.; Bartlett, R. J. A Direct Product Decomposition Approach for Symmetry Exploitation in ManyBody Methods. I. Energy Calculations. *J. Chem. Phys.* **1991**, *94*, 4334−4345.
(65) Gauss, J.; Stanton, J. F. Coupled-Cluster Calculations of Nuclear Magnetic Resonance Chemical Shifts. *J. Chem. Phys.* **1995**, *103*, 3561−3577.
(66) Gordon, R. G. Molecular Motion in Infrared and Raman Spectra. *J. Chem. Phys.* **1965**, *43*, 1307−1312.
(67) McQuarrie, D. A. *Statistical Mechanics; Harper's Chemistry Series*; HarperCollins Publishing, Inc.: New York, 1976.
(68) Williams-Young, D. B.; Petrone, A.; Sun, S.; Stetina, T. F.; Lestrange, P.; Hoyer, C. E.; Nascimento, D. R.; Koulias, L.; Wildman, A.; Kasper, J.; Goings, J. J.; Ding, F.; DePrince, A. E.; Valeev, E. F.; Li, X. The Chronus Quantum (ChronusQ) Software Package. *Wiley Interdiscip. Rev.: Comput. Mol. Sci.* **2019**, DOI: 10.1002/wcms.1436.
(69) Calvin, J. A.; Valeev, E. F. TiledArray: A general-purpose scalable block-sparse tensor framework. https://github.com/valeevgroup/tiledarray (2019).
(70) Francl, M. M.; Pietro, W. J.; Hehre, W. J.; Binkley, J. S.; Gordon, M. S.; DeFrees, D. J.; Pople, J. A. Self-consistent molecular orbital methods. XXIII. A polarization-type basis set for second-row elements. *J. Chem. Phys.* **1982**, *77*, 3654.
(71) Gordon, M. S.; Binkley, J. S.; Pople, J. A.; Pietro, W. J.; Hehre, W. J. Self-consistent molecular-orbital methods. 22. Small split-valence basis sets for second-row elements. *J. Am. Chem. Soc.* **1982**, *104*, 2797.
(72) Rassolov, V. A.; Ratner, M. A.; Pople, J. A.; Redfern, P. C.; Curtiss, L. A. 6-31G* basis set for third-row atoms. *J. Comput. Chem.* **2001**, *22*, 976.
(73) Bruner, A.; LaMaster, D.; Lopata, K. Accelerated Broadband Spectra Using Transition Dipole Decomposition and Pade Approximants. *J. Chem. Theory Comput.* **2016**, *12*, 3741−3750.
(74) Kramida, A.; Ralchenko, Y.; Reader, J.; NIST ASD Team *NIST Atomic Spectra Database* (version 5.6.1). National Institute of Standards and Technology, Gaithersburg, MD. https://physics.nist.gov/asd (2018).
(75) Goings, J. J.; Ding, F.; Frisch, M. J.; Li, X. Stability of the complex generalized Hartree-Fock equations. *J. Chem. Phys.* **2015**, *142*, 154109.
(76) Noro, T.; Sekiya, M.; Koga, T. Segmented Contracted Basis Sets for Atoms H Through Xe: Sapporo-(DK)-nZP Sets (n = D, T, Q). *Theor. Chem. Acc.* **2012**, *131*, 1124.
(77) Stetina, T. F.; Kasper, J. M.; Li, X. Modeling $L_{2,3}$-Edge X-ray Absorption Spectroscopy with Linear Response Exact Two-Component Relativistic Time-Dependent Density Functional Theory. *J. Chem. Phys.* **2019**, *150*, 234103.

DOI: 10.1021/acs.jctc.9b00729
J. Chem. Theory Comput. 2019, 15, 6617−6624